

Chapter 5

Extrinsic Defect Reactions in Perovskite Materials

The work presented in this Chapter has been published in *Solid State Ionics* [203].

5.1 Introduction

With dwindling fossil fuel reserves [204] and increasing awareness of global warming [205, 206], attention is being directed towards renewable and non-polluting energy systems. Many schemes are presently receiving attention: wind power [207], hydroelectric [208], solar [209], nuclear [210] and oxygen conduction [211]. The Kyoto protocol [171] was created to set targets for industrialised nations to cut their greenhouse gas emissions. As part of this drive for a non-polluting, energy efficient energy system, solid oxide fuel cells (SOFCs) are being investigated with great

fervour [212–216].

The most common types of fuel cells are phosphoric acid (PAFC), molten carbonate (MCFC), proton exchange membrane (PEMFC), and solid oxide (SOFC), all named after their electrolytes. As they are made of different materials and operating temperatures, they have varying benefits, applications and challenges, but all share the potential for high electrical efficiency and low emissions [96].

A schematic of a SOFC can be seen in Figure 5.1. SOFCs are electrochemical devices that convert hydrogen from the fuel directly into electricity and heat. The reaction is driven by the continual flow of oxygen ions (O^{2-}) across an electrolyte from the cathode to the anode. At the anode, these oxygen ions combine with the hydrogen to form water (H_2O) with the release of two electrons to an external circuit. A SOFC will also utilize any carbon in the fuel (CO), which makes them more versatile when using fuels such as natural gas or propane [96, 217]. When methane (CH_4) is used as the fuel source, this is internally reformed at the SOFC anode [218]. In the case where the fuel is CO , the O^{2-} ions oxidise CO to CO_2 . The two possible reactions at the anode (dependent on fuel) are therefore:



with the corresponding reaction at the cathode:



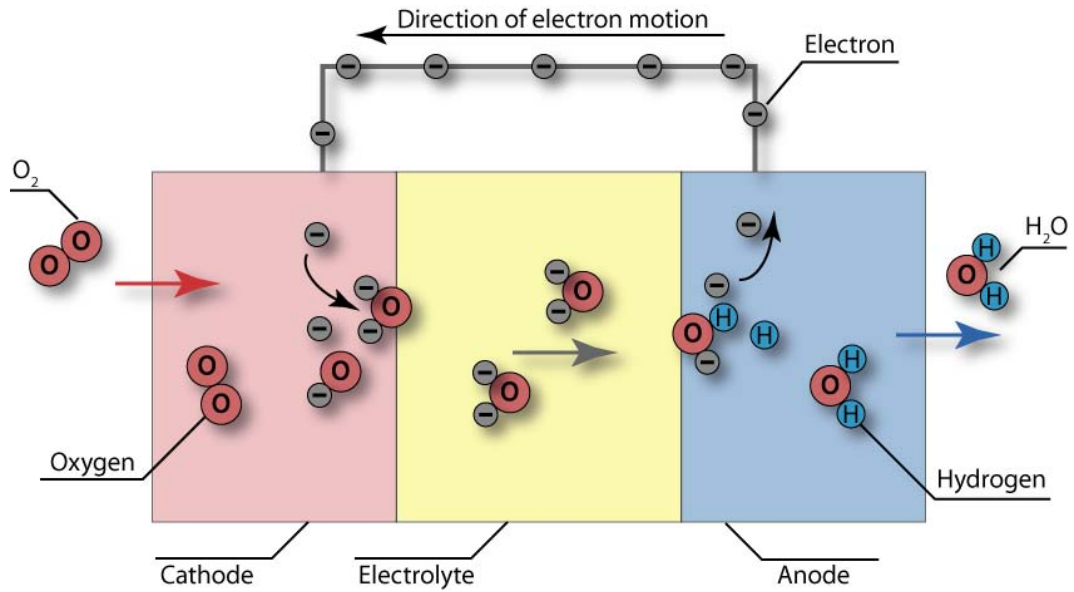


Figure 5.1: Schematic of a solid oxide fuel cell.

The total electrical conductivity (σ) of a solid is the sum of the partial conductivities of the ionic and electronic charge carriers [219]:

$$\sigma = \sum q_i \mu_i c_i \quad (5.3)$$

where q_i is the charge, μ_i is the mobility and c_i is the density of the carriers. The conductivity can be raised by increasing the carrier concentration and/or increasing the mobility of the carriers. The mobility of the charge carriers is dependent upon temperature, composition and processing (grain boundaries, dislocations etc.). The carrier concentration can be altered in two ways. Firstly, the material can be doped with aliovalent impurities that require the formation of ionic defects to maintain charge neutrality [219], or secondly, by deviations from ideal stoichiometry, i.e. either the oxidation or reduction of the material resulting in excess vacancies or interstitials [219]. For the purpose of this work, only the case where the materials

are doped was investigated.

One of the major technological problems with SOFCs is that in order to achieve high electrical conductivities they must operate at high temperatures. Currently, the best SOFCs use a doped zirconia electrolyte and in order to obtain the optimum performance from such cells they must be operated at temperatures greater than 800°C [220]. This exacerbates mechanical problems such as thermal fatigue and limits the choice of materials for interconnects and seals and necessitates the use of expensive alloys [220]. Consequently there is a drive to develop SOFC electrolytes with higher conductivities at lower temperatures [217]. $\text{Ce}_{0.9}\text{Gd}_{0.1}\text{O}_{1.95}$ is being enthusiastically developed since it yields a comparable conductivity at only 500°C [96]. These next generation SOFCs are therefore known as intermediate temperature SOFCs (IT-SOFCs).

At the present time much attention is focused on oxides with perovskite structures with the expectation of developing better cathodes [96]. It is known that ABO_3 materials such as LaCoO_3 [221] and LaInO_3 [214] can accommodate large concentrations of anion vacancies which lead to high oxygen conductivities. However, when considering the case where both the A and B cations adopt formal 3+ valance states, it is necessary to impose divalent cation substitution to increase the population of mobile oxygen vacancies. For example, in the case of LaCoO_3 , Sr^{2+} is doped onto the La^{3+} site in order to increase the oxygen conductivity [215]. The majority of perovskite-type oxides currently in use are based on either $\text{La}_{1-x}\text{Sr}_x\text{CoO}_{3-\delta}$ or $\text{La}_{1-x}\text{Sr}_x\text{MnO}_{3-\delta}$, however, $\text{Sm}_{1-x}\text{Sr}_x\text{CoO}_{3-\delta}$ has been shown to have considerable promise [220]. The choice of divalent cation substitution is, however, expected to depend on the host lattice composition.

Another perovskite, Sr^{2+} doped LaGaO_3 , is attracting attention as a potential

electrolyte for IT-SOFCs. Despite it having a slightly lower conductivity than $\text{Ce}_{0.9}\text{Gd}_{0.1}\text{O}_{1.95}$, it is able to operate over a wider temperature range (e.g. at 600°C where the reduction of Ce^{4+} occurs). A concern with this material, however, is the garnet dissociation reaction as described in Chapter 3, which manifests itself as second phases of $\text{SrLaGa}_3\text{O}_7$ and $\text{La}_4\text{Ga}_2\text{O}_9$ often at the grain boundaries [96]. Similar stability problems have also been found with the use of $\text{La}_{0.9}\text{Sr}_{0.1}\text{Ga}_{0.8}\text{Mg}_{0.2}\text{O}_{2.85}$. Other than altering composition or increasing temperature, the conductivity can be improved by creating thin film electrolytes, although these become very fragile and difficult to handle.

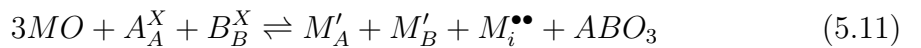
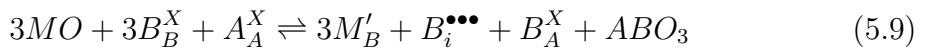
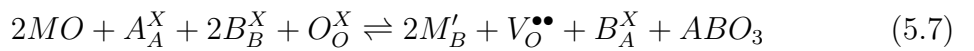
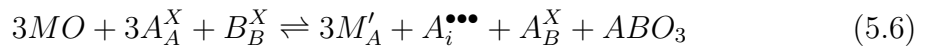
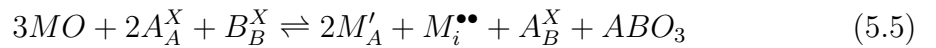
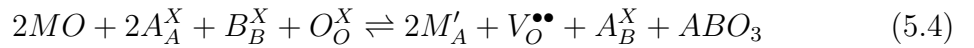
The focus of the present study was to investigate the interplay of the crystallography and doping in a subset of perovskite materials where both the A and B cations adopt formal 3+ valence states. Solution of Ba^{2+} , Ca^{2+} , Cd^{2+} , Co^{2+} , Mg^{2+} and Sr^{2+} into the Pnma and P6₃cm variants of ABO_3 materials was considered (see Chapter 3 for details of the crystallography).

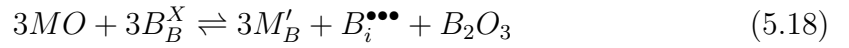
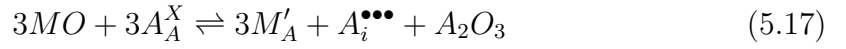
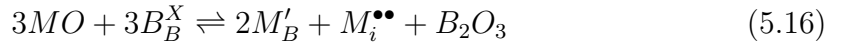
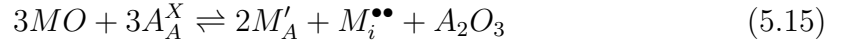
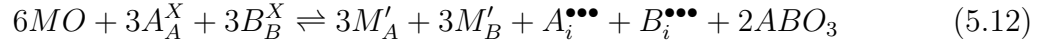
5.2 Defect Equilibria

Incorporation of a divalent cation onto a trivalent cation lattice site results in a charge imbalance that requires charge compensation by another lattice defect. There are three potential compensating defects: (i) a host lattice oxygen vacancy (Equations 5.4, 5.7, 5.10, 5.13 and 5.14), (ii) a dopant (2+) interstitial ion (Equations 5.5, 5.8, 5.11, 5.15 and 5.16) or (iii) a lattice self interstitial cation (Equations 5.6, 5.9, 5.12, 5.17 and 5.18). The oxygen vacancy and host interstitial mechanisms are related through the Schottky and cation Frenkel equilibria. In all equations, site and charge balance is maintained, and in Equations 5.4 to 5.12 the A:B ratio of ABO_3 is

also maintained. However, in Equations 5.13 to 5.18 the doping introduces a level of nonstoichiometry with the formation of second phase material in the form of A_2O_3 or B_2O_3 .

These various mechanisms were derived as follows. Initially, if only the case where the material remains stoichiometric is considered, three outcomes are possible. Firstly, the divalent cation can dissolve onto a lattice A site (Equation 5.4), secondly onto a lattice B site (Equation 5.7), and thirdly it can dissolve onto both sites simultaneously (Equation 5.10). Reactions of these types involve the formation of excess ABO_3 lattice (via the formation of a cation antisite defect). If a stoichiometric ratio is no longer maintained, divalent ion solution onto the lattice A site can also be facilitated by a reaction in which excess A_2O_3 is formed (Equation 5.13). Equivalently, when solution is onto the lattice B site, a reaction is possible in which excess B_2O_3 is formed (Equation 5.14). Second phase formation will generally lead to the detriment of transport and electrical properties due to associated inhomogeneities.





It is also possible for the dopant ion to dissolve onto an interstitial site with charge compensation via an oxygen interstitial defect ($MO + O_O^X \rightleftharpoons M_i^{\bullet\bullet} + O_i''$). However, reactions of this type involving oxygen excess nonstoichiometry have not been considered as the inclusion of oxygen interstitial defects into the lattice is a very high energy process (see Chapter 4).

In this study, the divalent cations being dissolved into the lattice were; Ba^{2+} , Ca^{2+} , Cd^{2+} , Co^{2+} , Mg^{2+} and Sr^{2+} . These represent common dopants used in the design of SOFC materials and have a range of ionic radii (0.89 to 1.42 Å) suitable for the perovskite compounds considered here.

Solution mechanisms were compared by generating graphs that detail solution energy (the internal energy) as a function of the radius of the dopant ion. Since the A and B lattice sites have different coordinations, an effective dopant ion radius with an intermediate coordination of eight (taken from Shannon [30]) has been chosen to facilitate this comparison. In all cases the energies reported are for the complete solution reaction normalised per defect as dictated by a mass action analysis (this

approach has been reported in detail previously [3,222]; further details are given in Appendix A).

Solution of MO via Equation 5.4 requires knowledge of the lattice energies of MO and ABO_3 , the incorporation defect energy of a substitutional M ion at an A lattice site, an A cation at a B lattice site, and the energy to form an oxygen vacancy. These were summed as dictated by equation 5.4 and it was noted that the energy of the defects such as A_A^X , B_B^X and O_O^X are zero. Energies for other solution reactions were obtained equivalently.

5.3 Results and Discussion

Solution of the divalent cations Ba^{2+} , Ca^{2+} , Cd^{2+} , Co^{2+} , Mg^{2+} and Sr^{2+} are shown in Figures 5.2 to 5.5. The solution reactions listed above in Section 5.2 are shown according to the key and can be built up by colour, symbol and line style. The VIII coordinate cation radii of the six dopant ions is shown in Table 5.1.

Table 5.1: VIII co-ordinate effective cation radii for the divalent dopant ions [30].

Cation	Effective ionic radius Å
Mg^{2+}	0.89
Co^{2+}	0.90
Cd^{2+}	1.10
Ca^{2+}	1.12
Sr^{2+}	1.26
Ba^{2+}	1.42

From Figures 5.2 to 5.5 it is evident that there are several general trends for solution of divalent ions into the four compositions. The lowest energy solution process (most

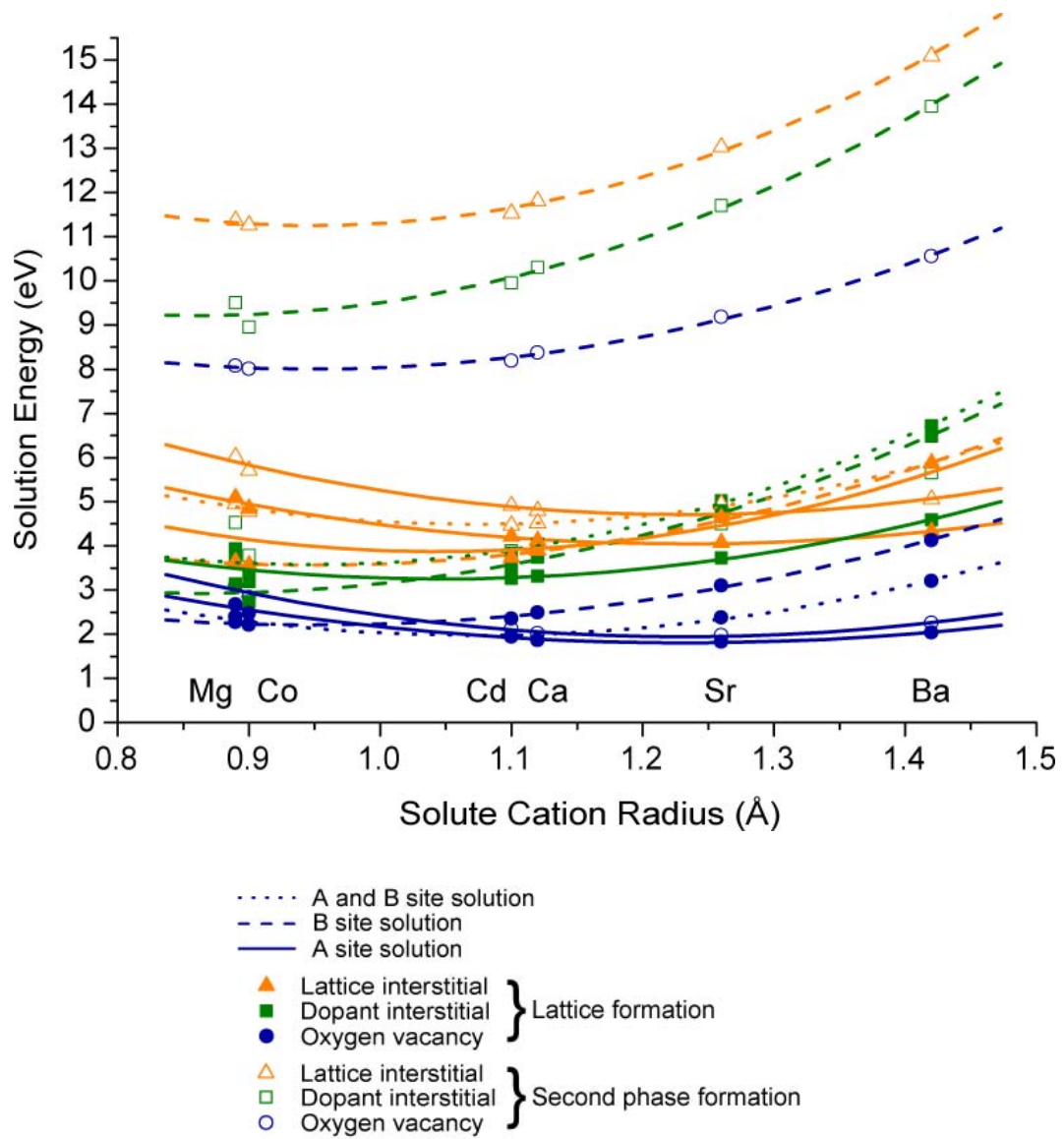


Figure 5.2: Divalent cation solution into LaScO₃. Note that the reference radii are La³⁺ = 1.16 Å, Gd³⁺ = 1.053 Å, Sc³⁺ = 0.87 Å and In³⁺ = 0.92 Å.

favourable) is that where the charge compensating defect is an oxygen vacancy. The lowest energy processes are also those where the perovskite remains stoichiometric (Equations 5.4, 5.7 and 5.10). Second phase formation will generally lead to detrimental transport and electrical properties of the material due to associated in-

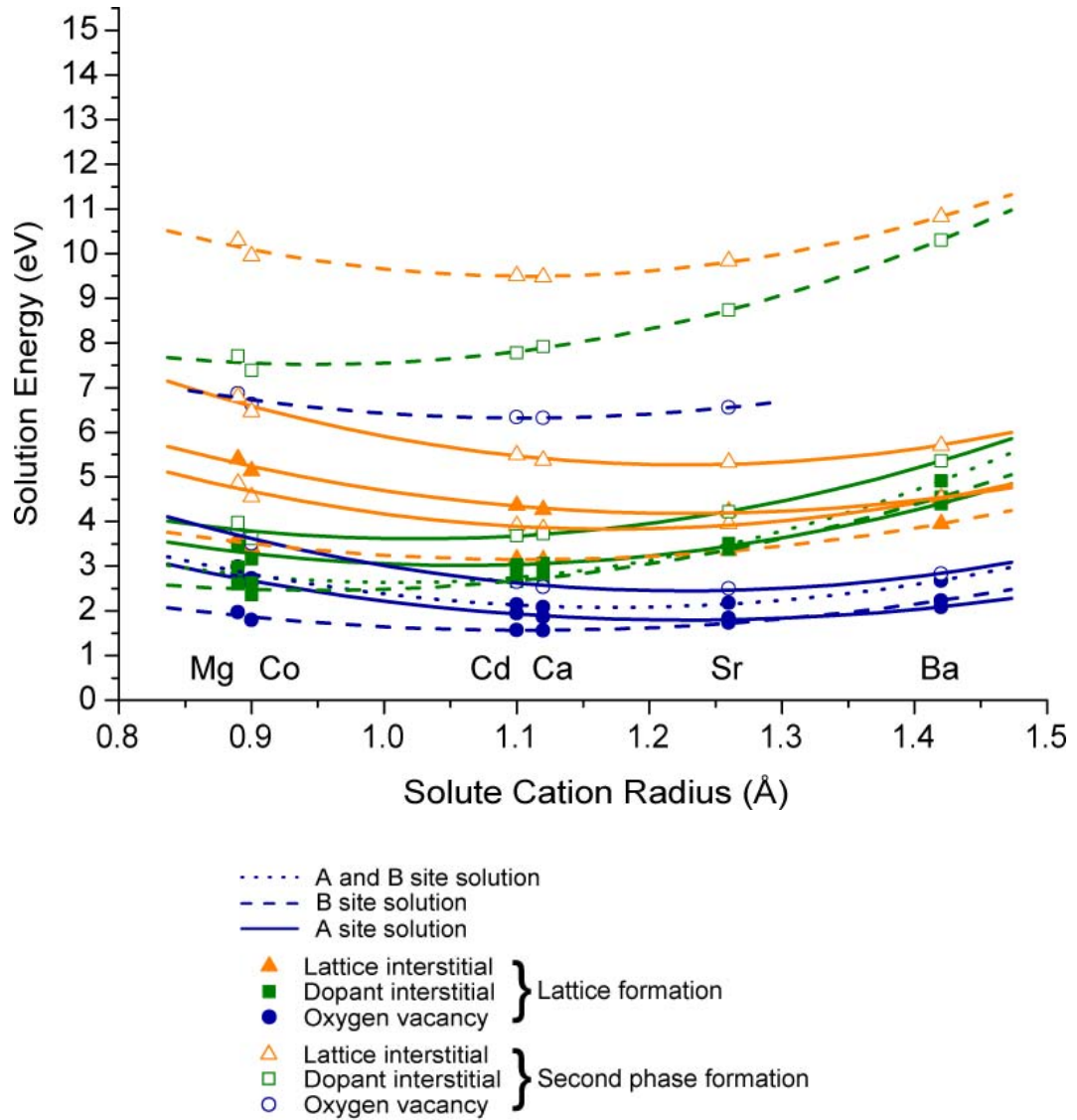


Figure 5.3: Divalent cation solution into LaInO₃. Note that the reference radii are La³⁺ = 1.16 Å, Gd³⁺ = 1.053 Å, Sc³⁺ = 0.87 Å and In³⁺ = 0.92 Å.

homogeneities. This trend for continued stoichiometry is therefore of benefit to the properties important for efficient application to SOFCs. It is also important to note that on doping these materials will form oxygen vacancies. Since these are important charge carriers for SOFC operation, divacancy doping is predicted to be an efficient doping process, in general agreement with experimental practice [223–225].

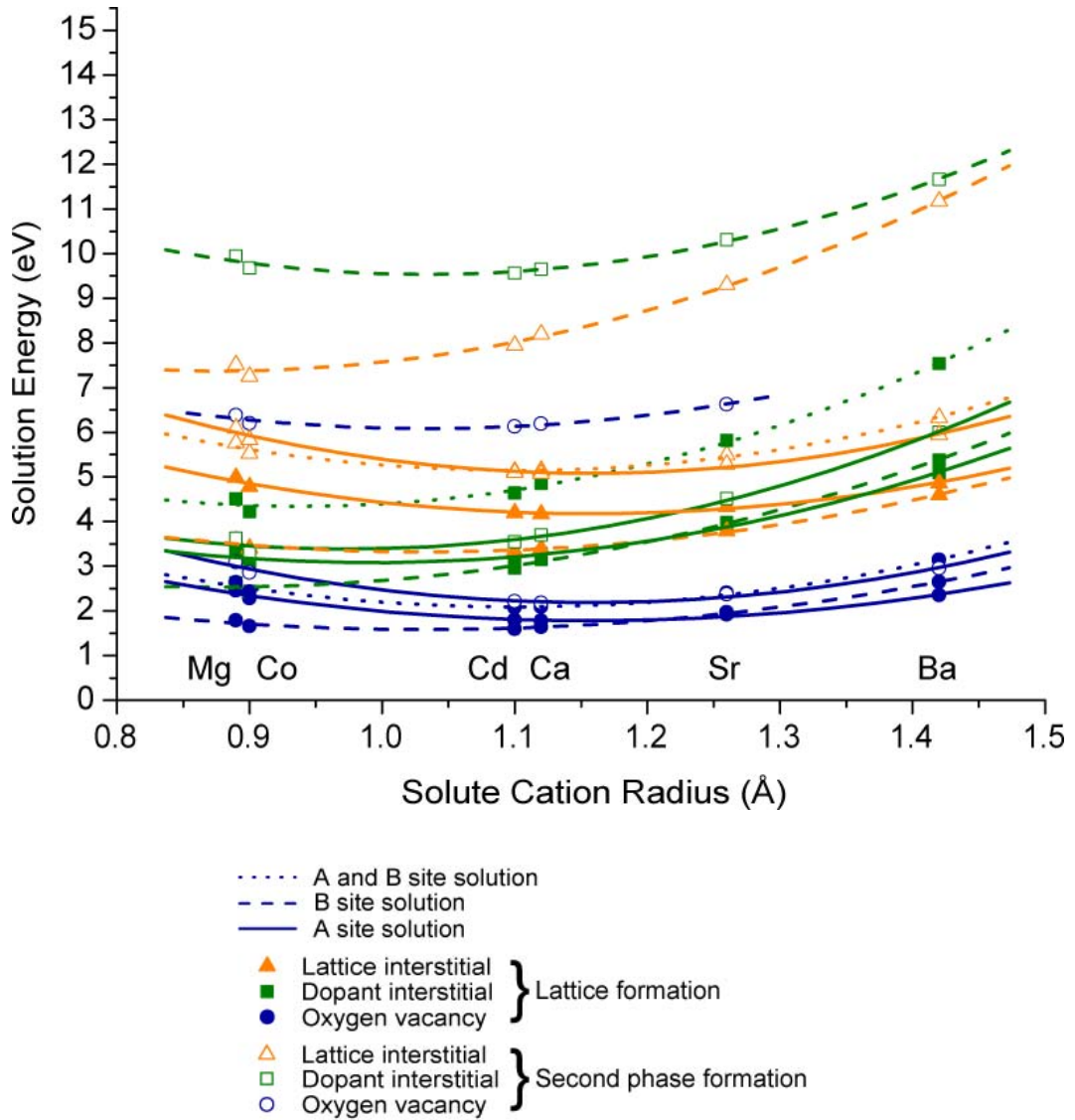


Figure 5.4: Divalent cation solution into GdScO₃. Note that the reference radii are La³⁺ = 1.16 Å, Gd³⁺ = 1.053 Å, Sc³⁺ = 0.87 Å and In³⁺ = 0.92 Å.

Of the four host lattices considered, LaScO₃ exhibits the highest overall reaction energies for solution onto the B lattice site with the formation of B₂O₃. LaScO₃ is the only orthorhombic (pnma) compound considered here, but it may follow that this very high energy for solution onto the B lattice site is a consequence of the host lattice crystallography. In the orthorhombic lattice, the A and B lattice sites

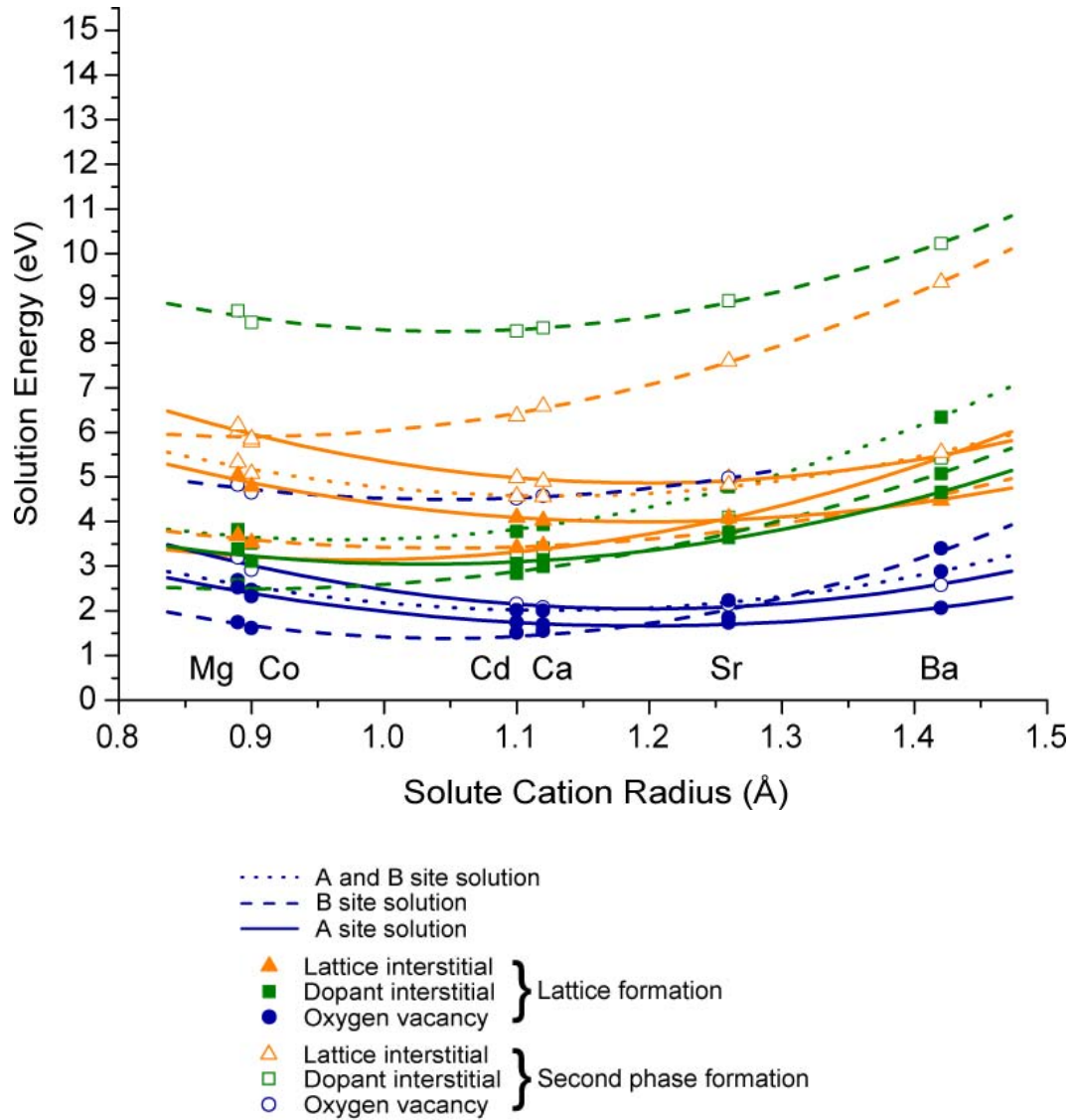


Figure 5.5: Divalent cation solution into GdInO₃. Note that the reference radii are La³⁺ = 1.16 Å, Gd³⁺ = 1.053 Å, Sc³⁺ = 0.87 Å and In³⁺ = 0.92 Å.

are 12 and 6 fold coordinated by oxygen, therefore, the B cation is located in the center of a BO₆ octahedra which is the smallest lattice site. Although the situation is similar for the hexagonal (P6₃cm) compounds, for these, the A and B lattice sites are 7 and 5 fold coordinated, the B lattice site is still smaller than the A site, but the difference is not so marked as for the orthorhombic lattice. This trend is shown

in the solution results, for example, on comparing Figures 5.2 and 5.3 it is evident that the maximum energy processes are of a far higher value for the orthorhombic phase than the hexagonal.

The relative solution energies for the three hexagonal ($P6_3cm$) materials ($LaInO_3$, $GdScO_3$ and $GdInO_3$) are similar. There are minor variations which are due to differences in the A and B cation radii, but the magnitude of the reactions is much more similar than in comparison to the orthorhombic $LaScO_3$.

In order to elucidate trends in the competing lowest energy reactions, it is necessary to consider only these lowest energy processes in more depth. Therefore, the solution reactions involving charge compensation via an oxygen vacancy are shown in Figures 5.6 to 5.9.

The general trend for the divalent solution in the four compounds is that smaller dopants (e.g. Mg^{2+}) substitute onto the smaller B lattice site, while larger dopants (e.g. Ba^{2+}) substitute onto the larger A lattice site. There is, however, a distinct difference in the solution site preference between the orthorhombic and hexagonal compounds. For the orthorhombic $LaScO_3$, the smallest of the dopants, Mg^{2+} and Co^{2+} , substitute onto the small B lattice site (Equation 5.7). At a solute cation radius of approximately 0.92 \AA the lowest energy solution site changes so that solution is preferred on both the A and B lattice sites (Equation 5.10). When the solute cation radius reaches 1.1 \AA , the site preference changes again, and ions larger than Cd^{2+} substitute onto the larger A lattice site (Equation 5.4).

For the hexagonal compounds the case is different; although smaller dopants again substitute onto the B lattice site, there is now no intermediate stage, and the larger dopant ions substitute only onto the A lattice site. The explanation for this is that

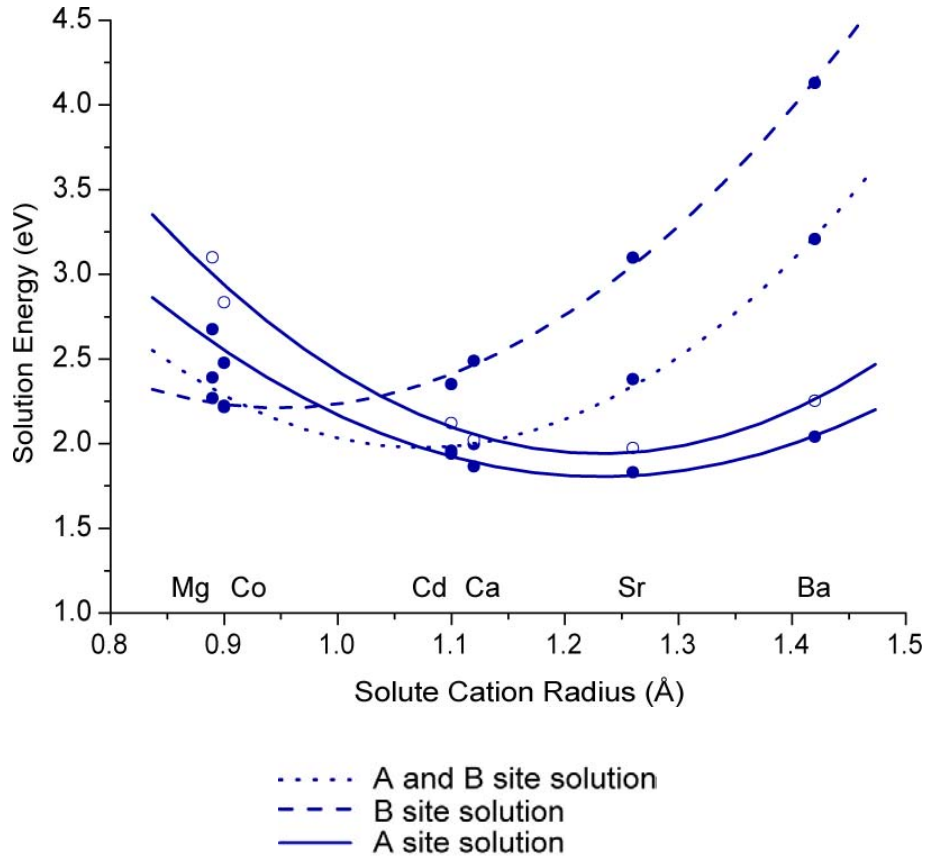


Figure 5.6: Lowest energy mechanisms for divalent cation solution into LaScO_3 . Note that the reference radii are $\text{La}^{3+} = 1.16 \text{ \AA}$, $\text{Gd}^{3+} = 1.053 \text{ \AA}$, $\text{Sc}^{3+} = 0.87 \text{ \AA}$ and $\text{In}^{3+} = 0.92 \text{ \AA}$.

the A and B lattice sites in the hexagonal materials are more comparable in size than those in the orthorhombic materials. This is due to the underlying crystallography, whereby in the hexagonal ($P6_3cm$) materials the A and B lattice sites are 7 and 5 coordinated by oxygen, whereas in the orthorhombic materials the A and B lattice sites are 12 and 6 fold coordinated by oxygen.

GdScO_3 is the compound with the smallest A and B cations that adopts the hexagonal $P6_3cm$ symmetry. For the small to intermediate cation radii dopants, (Mg^{2+} ,

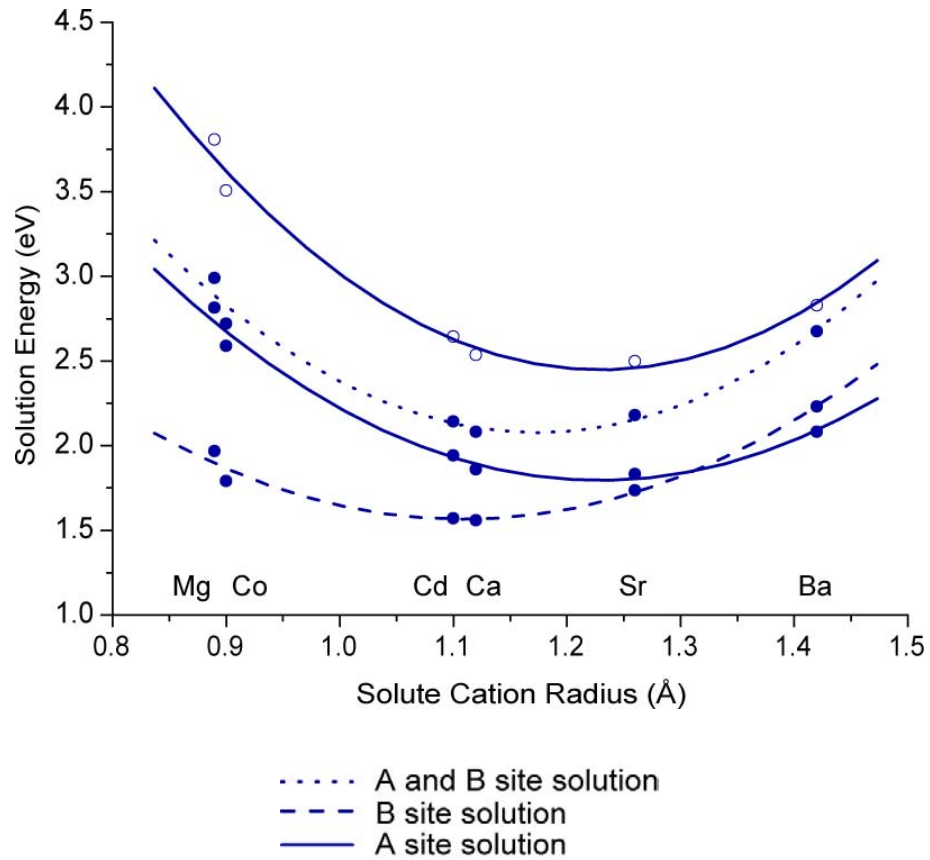


Figure 5.7: Lowest energy mechanisms for divalent cation solution into LaInO_3 . Note that the reference radii are $\text{La}^{3+} = 1.16 \text{ \AA}$, $\text{Gd}^{3+} = 1.053 \text{ \AA}$, $\text{Sc}^{3+} = 0.87 \text{ \AA}$ and $\text{In}^{3+} = 0.92 \text{ \AA}$.

Co^{2+} , Cd^{2+} and Ca^{2+}) solution is preferred onto the smaller B lattice site. It is also in this region of the graph that the overall minimum in solution energy occurs; at 1.04 \AA the energy reaches a minimum of 1.3 eV , the closest dopant to this minimum is Cd^{2+} , with a radius of 1.1 \AA . At a dopant radius of 1.2 \AA , there is a change in preference in the solution site to solution onto the larger lattice A site, therefore Sr^{2+} and Ba^{2+} substitute onto the A lattice site.

Concentrating on the Gd^{3+} containing compounds and maintaining the hexagonal

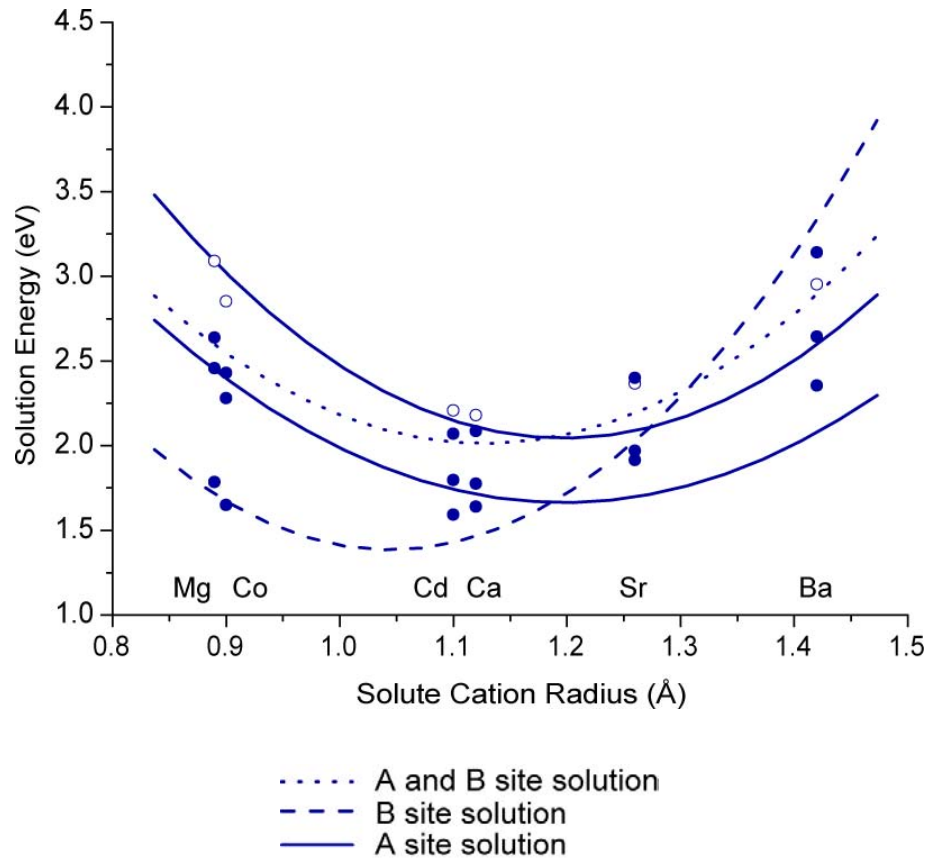


Figure 5.8: Lowest energy mechanisms for divalent cation solution into GdScO₃. Note that the reference radii are La³⁺ = 1.16 Å, Gd³⁺ = 1.053 Å, Sc³⁺ = 0.87 Å and In³⁺ = 0.92 Å.

crystallography, it is now pertinent to consider solution into GdInO₃. The trend is very similar to GdScO₃, with Mg²⁺, Co²⁺, Cd²⁺ and Ca²⁺ substituting onto the smaller B lattice site, and Sr²⁺ and Ba²⁺ substituting onto the A lattice site. The minimum in the solution energy is also very similar, 1.3 eV at a solute cation radius of 1.04 Å. The change in preference between solution onto the B and A lattice sites again occurs at a dopant radii of 1.2 Å.

If attention is now drawn to the remaining hexagonal compound, LaInO₃, it is clear

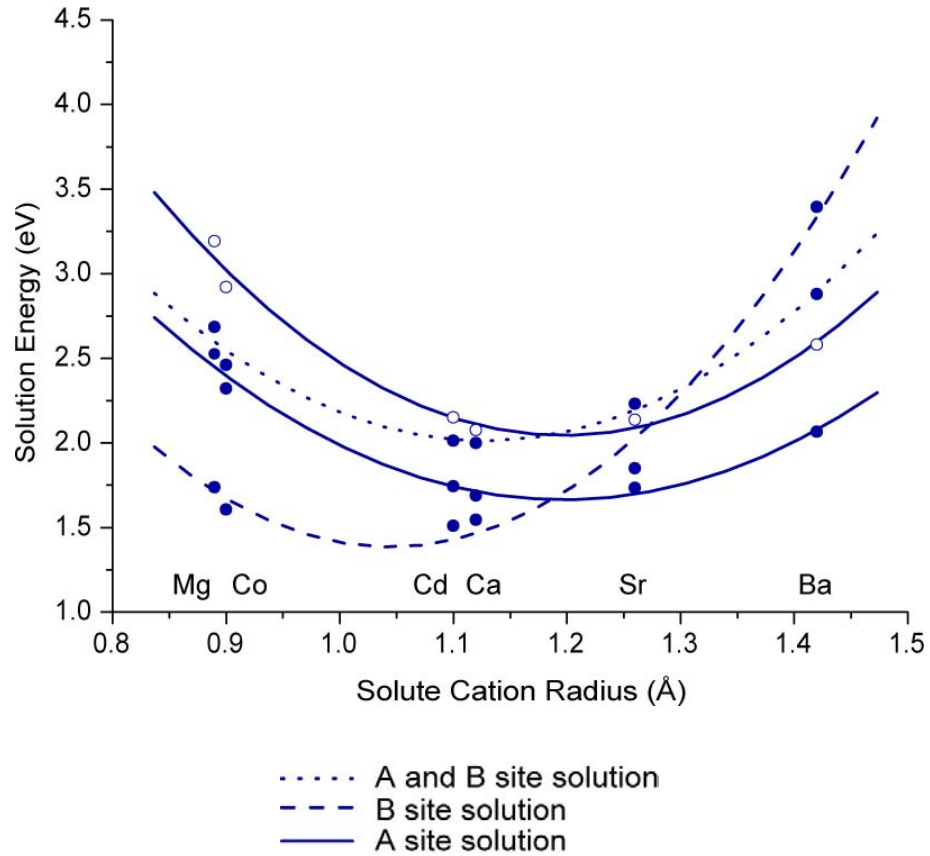


Figure 5.9: Lowest energy mechanisms for divalent cation solution into GdInO₃. Note that the reference radii are La³⁺ = 1.16 Å, Gd³⁺ = 1.053 Å, Sc³⁺ = 0.87 Å and In³⁺ = 0.92 Å.

that there is a difference from the trend seen with the Gd³⁺ containing compounds. Here, the smaller dopant cations again substitute onto the B lattice site, however the change over in preference for this solution site occurs at a much higher solute cation radius. Here, Mg²⁺, Co²⁺, Cd²⁺, Ca²⁺ and Sr²⁺ substitute onto the B lattice site, with only Ba²⁺ substituting onto the A lattice site. Thus this change of preference occurs at the larger dopant cation radius of 1.32 Å. The overall minimum in solution energy is 1.52 eV and this occurs for Ca²⁺ (1.12 Å) solution onto the B lattice site.

The situation is different for the orthorhombic compound LaScO_3 . Here only the smallest dopant cations (Mg^{2+} and Co^{2+}) substitute onto the B lattice site with all larger dopants (Cd^{2+} , Ca^{2+} , Sr^{2+} and Ba^{2+}) substituting onto the larger A lattice site. However, between Co and Cd in a solute cation range from 0.92 Å to 1.09 Å, solution is preferred on a combination of both the A and B lattice sites. This is a marked difference from the hexagonal materials since for these, solution onto the A and B lattice sites simultaneously is far less favourable than solution fully onto the A or B lattice sites individually for any solute cation. A further difference can be seen between LaScO_3 and the hexagonal materials, in that the minimum in solution energy occurs at a much higher solute cation radii (1.25 eV which corresponds to Sr^{2+} solution) and for a domain of the graph whereby solution is preferred onto the lattice A site, this minimum is also a higher energy than that for any of the hexagonal materials at 1.77 eV.

Despite the differences in solution energy, the trends between the three hexagonal materials are the same. For these hexagonal materials the minimum in the solution energy occurs at a solute cation radius that seems to be governed somewhat by the lattice A cation size. When GdScO_3 and GdInO_3 are compared, this minimum in solution energy occurs at the same point (solution cation radius of 1.04 Å) and the change in solution site preference also occurs at the same point (solute cation radius of 1.2 Å). However, when GdInO_3 and LaInO_3 are compared, both the minimum and change in solution site preference are shifted to larger solute cation radii (1.12 Å and 1.32 Å respectively). This reflects the increase in A cation size in the host lattice from Gd (1.053 Å) to La (1.16 Å).

The overall minimum in solution energy across all four compounds is for Cd^{2+} solution onto the B lattice site of GdInO_3 . The next lowest solution is for Cd^{2+}

solution into GdScO_3 , with Cd^{3+} solution into LaInO_3 and Sr^{2+} solution into LaScO_3 being higher still.

5.4 Conclusions

The mechanisms by which divalent ions are accommodated in ABO_3 perovskite materials have been identified by predicting solution energies as a function of dopant ion radius. For all four materials studied, these dopants are always charge compensated by oxygen vacancies. Furthermore, the smallest dopants will substitute on B sites and the largest on A sites. However, the dopant radius at which this change in lattice site preference occurs is a function of both lattice composition and crystallography.

Due to this crystallography condition for solution, the orthorhombic compound is more sensitive to solution site than the hexagonal materials. This is a result of the relative sizes of the A and B lattice sites, which in turn is related to the coordination of those sites. In the orthorhombic structure, the A and B sites are 12 and 6 fold coordinated by oxygen, and in the hexagonal material they are 7 and 5 fold coordinated by oxygen. Therefore the sites in the hexagonal materials are more similar in size than those in the orthorhombic material. This leads to only very small dopants substituting at the B lattice site, followed by an intermediate step whereby solution is facilitated onto both lattice cation sites, and finally larger cations substituting onto the large A site in the orthorhombic material. In the hexagonal materials, a majority of the dopants substitute onto the B lattice site, with only the largest substituting onto the A lattice site, and with no intermediate step.

A further consequence of this crystallographic variation is that the energy is higher for solution into the orthorhombic LaScO_3 than into the three hexagonal compounds (LaInO_3 , GdScO_3 and GdInO_3). Therefore, the concentration of oxygen vacancies that would be formed is lower in the LaScO_3 than in the other compositions.

For the hexagonal materials, changes in the B site chemistry do not affect the doping scheme significantly. However chemistry changes on the A site do affect the doping schedule, as can be seen from comparison of GdScO_3 with GdInO_3 , and GdInO_3 with LaInO_3 .

For efficient SOFC operation, a high concentration of oxygen vacancies is required. The highest defect concentration occurs for the lowest solution energy. Therefore, the lower the solution energy, the more dopant will dissolve into the material, and the more charge compensating oxygen vacancies are formed. With this knowledge, it would seem that the hexagonal material, $\text{GdIn}_{1-x}\text{Cd}_x\text{O}_3$ would be the best choice for use in SOFCs. Of course, other criteria such as chemical compatibility with other materials in the system are also important. Nevertheless, the work shown here provides a useful approach for directing future research on SOFC systems.